Eurographics Symposium on Geometry Processing 2011
Mario Botsch and Scott Schaefer
(Guest Editors)

Volume 30 (2011), Number 5

Rational bi-cubic G^2 splines for design with basic shapes

Kęstutis Karčiauskas[1] and Jörg Peters[2]

[1]Vilnius University [2]University of Florida

Abstract

The paper develops a rational bi-cubic G^2 (curvature continuous) analogue of the non-uniform polynomial C^2 cubic B-spline paradigm. These rational splines can exactly reproduce parts of multiple basic shapes, such as cyclides and quadrics, in one by default smoothly-connected structure. The versatility of this new tool for processing exact geometry is illustrated by conceptual design from basic shapes.

Categories and Subject Descriptors (according to ACM CCS): I.3.5 [Computer Graphics]: Curve, surface solid and object representation—Splines

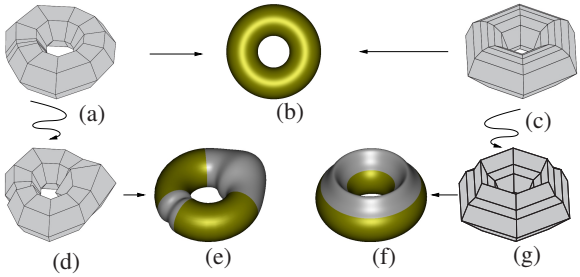

Figure 1: *Both the meshes (a) and (c) map to the exact torus (b) represented as a piecewise rational spline of degree bi-3 (bi-cubic). The two different mesh structures allow for different designs: (a) is geometrically modified to (d) yielding the bi-3 surface (e) and (c) is geometrically modified to (g) yielding the bi-3 surface (f). The golden components remain exactly on the torus.*

1. Introduction

This paper develops a rational G^2 spline analogue of the polynomial C^2 cubic B-spline paradigm to be able to include a sequence of approximate or exact rational primary shapes, such as tori, cyclides, spheres etc. and automatically combine them into a smooth whole. The new splines support ab initio design, re-design starting with CSG models or reconstruction in reverse engineering. We focus on use in conceptual design as illustrated in Fig. 1: a popular approach to conceptual design of outer surfaces is to start from primary shapes, such as quadrics or cyclides, that represent functionality or simplicity of shape, and modify them. Extending this way of thinking to implementation, however, creates challenges. When multiple pieces are created in isolation, as separate entities, they must be combined using intersections, fillets and blends. This complicates downstream manipulation, design refinement and analysis. This paper therefore proposes a class of curvature continuous rational splines that generalize C^2 splines in that they reproduce classical shapes without the need to, a posteriori, stitch the conceptual pieces together. Such built-in blending is useful when varying designs while preserving constraints as part of a shape optimization process.

Bi-cubic polynomial B-splines are well-known and widely used at all levels of geometry processing since they combine smoothness and flexibility with simplicity. However, even for the regular tensor-product layout, let alone in the presence of extraordinary points, designing surfaces as fair as the classical basic shapes, is a challenge. Moreover, for mechanical applications, for example for ball and socket joints, basic non-polynomial shapes have to be reproduced exactly. Rational geometric splines have been developed as early as [Boe87, GB88] and both [Joe89, Bar93] observe that the parameter β of first order geometric continuity can represent local knot spacing. This classical work is primarily interested in algebraic generality. It treats the many scalars of geometric continuity and rational weights as free parameters and does not provide constructive recipes. In our approach, all parameters are initialized to reproduce basic shapes and modifying them is entirely optional. Concerning shape reproduction, there are two approaches in the literature. The first, exemplified by modeling circles as projections of C^2

curves in homogeneous space, leads to high degree parameterizations, e.g. degree 6 for circles [BP97]. The second is to use rational pieces in Bernstein-Bézier form to model individual conic shapes; this lacks built-in smooth transitions. A concrete framework, that guarantees *both built-in smoothness and reproduction of multiple basic shapes* is missing in the literature. We now present such a framework, based on 4-tuples of rational G^2 splines of lowest possible bi-degree.

The structure of this paper is as follows. Section 2 specifies the construction of rational cubic G^2 spline curves that can reproduce basic curve shapes. Section 3 gives a tensoring procedure that yields rational bi-cubic G^2 splines capable of reproducing cyclides and tori. Section 5 adds spheres and sphere-like shapes to the toolkit. General, multi-sided blends fall outside the rational bi-3 G^2 paradigm and are not covered by this paper.

2. Rational Cubic G^2 Curves

When defining splines, here first in one variable, we make use both of a B-spline-like control polygon with points $\mathbf{p}^i$ and of functions f of degree 3 in rational Bernstein-Bézier form to represent curve segments. For example, with $u \in [0..1]$ (cf. [Far88, PBP02] for canonical expositions)

$$f(u) := \frac{\sum_{k=0}^3 w_k \mathbf{b}_k B_k(u)}{\sum_{k=0}^3 w_k B_k(u)}, \quad B_k(u) := \binom{3}{k}(1-u)^{3-k}u^k.$$

First we recall the notion of geometric continuity, i.e. matching of derivatives after reparameterization. This notion is central to our splines when we express them piecemeal in Bézier-form: it plays a role akin to non-uniform knot-spacing for standard splines.

Definition 1 (G^2 **continuity**) The maps $f : [0..1] \to \mathbb{R}$ and $g : [0..1] \to \mathbb{R}$ join G^1 at a common point $f(1) = g(0)$ if for some scalar $\beta > 0$

$$g'(0) = \beta f'(1), \tag{1}$$

and G^2 if additionally there exists $\gamma \in \mathbb{R}$

$$g''(0) = \beta^2 f''(1) + \gamma f'(1)\,. \tag{2}$$

We note that if f^{numer} and g^{numer} join G^2 with scalars β, γ and f^{denom} and g^{denom} join G^2 using the same scalars then $\frac{f^{numer}}{f^{denom}}$ and $\frac{g^{numer}}{g^{denom}}$ join G^2 with these parameters β, γ.

As illustrated in Fig. 2, the control structure of our rational cubic G^2 curves consist of

- the *affine* B-spline-like control points $\mathbf{p}^i \in \mathbb{R}^d$ ($d = 2$ for planar curves; we will also use $d = 1,3,4$);
- the parameters of G^2 continuity β_i,γ_i, associated with the junction of consecutive cubic segments f_{i-1} and f_i and
- the weights $w_k^i \in \mathbb{R}$ of maps f_i such that $w_3^{i-1} = w_0^i =: W_i$.

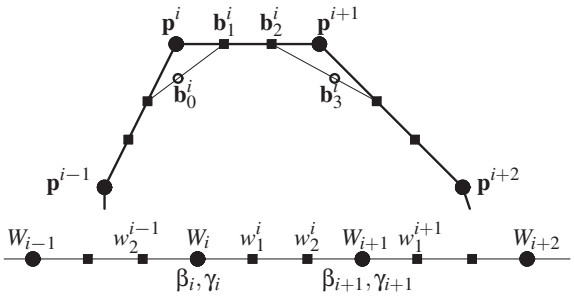

Figure 2: *The control structure of a rational cubic G^2 curve.*

From the control structure, we determine the affine coefficients $\mathbf{b}_k^i \in \mathbb{R}^d$,

$$\begin{aligned} \mathbf{b}_1^i &:= (1-t_i)\mathbf{p}^i + t_i\mathbf{p}^{i+1}\,,\ \mathbf{b}_2^i := \tilde{t}_i\mathbf{p}^i + (1-\tilde{t}_i)\mathbf{p}^{i+1}\,, \\ \mathbf{b}_0^i &:= (1-x_i)\mathbf{b}_2^{i-1} + x_i\mathbf{b}_1^i\,,\ \mathbf{b}_3^{i-1} := \mathbf{b}_0^i\,. \end{aligned} \tag{3}$$

$$\begin{aligned} l_i &:= -\frac{2W_i w_1^{i-1}(w_1^i + w_2^{i-1}\beta_i)\beta_i^2}{c_1\beta_i + c_2\beta_i^2 + c_3\gamma_i}\,, \quad \tilde{l}_i := \frac{w_2^i}{w_1^{i-1}\beta_i^2} l_i\,, \\ c_1 &:= 2w_2^{i-1}(3(w_1^i)^2 - W_i w_2^i - W_i w_1^i)\,, \\ c_2 &:= 2w_1^i(3(w_2^{i-1})^2 - W_i w_1^{i-1} - W_i w_2^{i-1})\,, \\ c_3 &:= w_1^{i-1} W_i w_1^i\,, \\ t_i &:= -\frac{\tilde{l}_i}{1 - l_{i+1} - \tilde{l}_i}, \tilde{t}_i := -\frac{l_{i+1}}{1 - l_{i+1} - \tilde{l}_i}, x_i := \frac{w_1^i}{w_2^{i-1}\beta_i + w_1^i}. \end{aligned} \tag{4}$$

The formulas (3) have the same structure as the standard conversion from B-spline to Bézier form. The additional flexibility guaranteeing reproduction and smoothness comes at the cost of the complex but explicit formulas (4). For polynomial C^2 splines, these formulas simplify since $w_k^i = 1$, $\gamma_i = 0$ and β_i is the ratio of the $i-1$st and ith knot interval.

With the help of symbolic computation, one can verify the following theorem.

Theorem 1 [KP, Thm 1] Let f_{i-1}, f_i be rational cubic curves with weights w_k^{i-1}, w_k^i and control points $\mathbf{b}_k^{i-1}$, $\mathbf{b}_k^i$ defined by (3). Then

$$f_i'(0) = \beta_i f_{i-1}'(1)\,,\ f_i''(0) = \beta_i^2 f_{i-1}''(1) + \gamma_i f_{i-1}'(1)\,.$$

Conversely, we can derive the control points $\mathbf{p}^i$ of the cubic G^2 spline curve from the Bézier-coefficients $\mathbf{b}_k^j$. As for C^2 splines, they are simply the intersections of lines through $\mathbf{b}_1^{i-1}, \mathbf{b}_2^{i-1}$ and $\mathbf{b}_1^i, \mathbf{b}_2^i$ (cf. Fig. 2 and Fig. 3 (a)).

Circular arcs. As illustrated in Fig. 3 (a), circle arcs f_i with opening angles α_i can be represented as rational cubic splines with G^2 continuity: we simply degree-raise their standard rational degree 2 representation, with end-weights

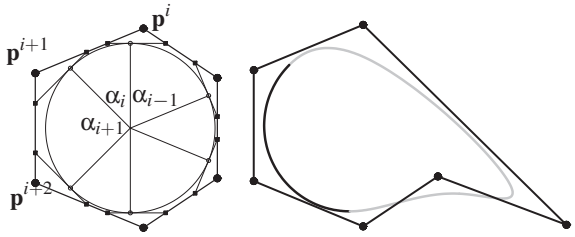

(a) circle (b) arc-preserving design

Figure 3: *Exact circle (a) defined from the asymmetric control polygon $\mathbf{p}^j$ as G^2 rational spline of degree 3. (b) Design variation that preserves circle arcs exactly (thick arcs).*

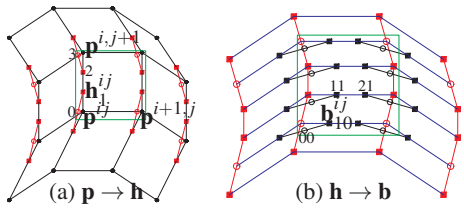

(a) $\mathbf{p} \to \mathbf{h}$ (b) $\mathbf{h} \to \mathbf{b}$

Figure 4: *Bi-cubic Construction*

equal to 1 and end-points $\mathbf{b}_3^{i-1} = \mathbf{b}_0^i$ on the circle [Far88] to obtain

$$f_i := \frac{\mathbf{b}_0^i B_0 + w\mathbf{b}_1^i B_1 + w\mathbf{b}_2^i B_2 + \mathbf{b}_3^i B_3}{B_0 + wB_1 + wB_2 + B_3}, \qquad (5)$$
$$w := \frac{1}{3} + \frac{2}{3}\cos\frac{\alpha_i}{2}.$$

This rational G^2 circle parameterization has scalars $\beta_i = \frac{\sin\frac{\alpha_i}{2}}{\sin\frac{\alpha_{i-1}}{2}}$, $\gamma_i = 2\beta_i\big(\tan\frac{\alpha_{i-1}}{4} + \tan\frac{\alpha_i}{4}\big)\sin\frac{\alpha_i}{2}$.
We will use (5) repeatedly to replace cos and sin expressions.

3. Bi-cubic Rational G^2 Splines

We obtain rules for a tensor-product spline surface essentially by tensoring the construction in Section 2. That is, we derive control points $\mathbf{b}_{rs}^{ij}$ and weights $w_{rs}^{ij} \in \mathbb{R}^d$ of the bi-cubic patches in Bernstein-Bézier form on the unit square

$$f^{ij}(u,v) := \frac{\sum_{r=0}^3\sum_{s=0}^3 w_{rs}^{ij}\mathbf{b}_{rs}^{ij}B_r(u)B_s(v)}{\sum_{r=0}^3\sum_{s=0}^3 w_{rs}^{ij}B_r(u)B_s(v)} \qquad (6)$$

from a regular quadrilateral grid of (B-spline-like) control points $\mathbf{p}^{ij} \in \mathbb{R}^d$ with associated scalars $\dot{w}_r^i, \dot{\beta}_i, \dot{\gamma}_i$ in the u-direction and scalars $\ddot{w}_s^j, \ddot{\beta}_j, \ddot{\gamma}_j$ in the v-direction.

Bi-cubic Construction: We set $w_{rs}^{ij} := \dot{w}_r^i\ddot{w}_s^j$ and compute the averaging quantities $\ddot{\iota}_j, \ddot{\tilde{\iota}}_j, \ddot{\chi}_j$ of (4) for one direction to get, as shown in Fig. 4, (a),

$$\mathbf{h}_1^{ij} := (1-\ddot{\iota}_j)\mathbf{p}^{ij} + \ddot{\iota}_j\mathbf{p}^{i,j+1}\ ,\ \mathbf{h}_2^{ij} := \ddot{\tilde{\iota}}_j\mathbf{p}^{ij} + (1-\ddot{\tilde{\iota}}_j)\mathbf{p}^{i,j+1}\ ,$$
$$\mathbf{h}_0^{ij} := (1-\ddot{\chi}_j)\mathbf{h}_2^{i,j-1} + \ddot{\chi}_j\mathbf{h}_1^{ij}\ ,\ \mathbf{h}_3^{i,j-1} := \mathbf{h}_0^{ij};\quad \text{(Fig. 4 (a))}$$

and then $\dot{\iota}_i, \dot{\tilde{\iota}}_i, \dot{\chi}_i$ to compute for the other direction

$$\mathbf{b}_{1s}^{ij} := (1-\dot{\iota}_i)\mathbf{h}_s^{ij} + \dot{\iota}_i\mathbf{h}_s^{i+1,j}\ ,\ \mathbf{b}_{2s}^{ij} := \dot{\tilde{\iota}}_i\mathbf{h}_s^{ij} + (1-\dot{\tilde{\iota}}_i)\mathbf{h}_s^{i+1,j}\ ,$$
$$\mathbf{b}_{0s}^{ij} := (1-\dot{\chi}_i)\mathbf{b}_{2s}^{i-1,j} + \dot{\chi}_i\mathbf{b}_{1s}^{ij}\ ,\ \mathbf{b}_{3s}^{i-1,j} := \mathbf{b}_{0s}^{ij}.\quad \text{(Fig. 4 (b))}$$

As in any tensoring procedure, the result is unchanged if we change which direction is first.

Theorem 2 The bi-cubic rational functions (6) defined by the Bi-cubic Construction form a G^2 spline complex.

Proof We show that

$$f_u^{ij}(0,v) = \dot{\beta}_i f_u^{i-1,j}(1,v)\ ,$$
$$f_{uu}^{ij}(0,v) = \dot{\beta}_i^2 f_{uu}^{i-1,j}(1,v) + \dot{\gamma}_i f_u^{i-1,j}(1,v).$$

By the symmetric argument $f_v^{ij}(u,0) = \ddot{\beta}_j f_v^{i,j-1}(u,1)$, $f_{vv}^{ij}(u,0) = \ddot{\beta}_j^2 f_{vv}^{i,j-1}(u,1) + \ddot{\gamma}_j f_v^{i,j-1}(u,1)$ then follows. By definition of the weights, $w_{rs}^{ij} := \dot{w}_r^i\ddot{w}_s^j$, and therefore

$$\sum_{r=0}^3\sum_{s=0}^3 w_{rs}^{ij}B_r(u)B_s(v) = \sum_{r=0}^3 \dot{w}_r^i B_r(u)\sum_{s=0}^3 \ddot{w}_s^j B_s(v)\ . \qquad (7)$$

Let j be fixed and define $\bar{w}_k(v) := \ddot{w}_k^j B_k(v)/\sum_{s=0}^3 \ddot{w}_s^j B_s(v)$. Then $\sum_{k=0}^3 \bar{w}_k(v) = 1$ and

$$f^{ij}(u,v) = \frac{\sum_{r=0}^3 \dot{w}_r^i\big(\sum_{s=0}^3 \bar{w}_s(v)\mathbf{b}_{rs}^{ij}\big)B_r(u)}{\sum_{r=0}^3 \dot{w}_r^i B_r(u)}.$$

With the abbreviations

$$\bar{\mathbf{b}}_{ir}(v) := \sum_{s=0}^3 \bar{w}_s(v)\mathbf{b}_{rs}^{ij} \quad\text{and}\quad \bar{\mathbf{p}}_i(v) := \sum_{s=0}^3 \bar{w}_s(v)\mathbf{p}_s^{ij},$$

$$f^{ij}(u,v) = \frac{\sum_{r=0}^3 \dot{w}_r^i\bar{\mathbf{b}}_{ir}(v)B_r(u)}{\sum_{r=0}^3 \dot{w}_r^i B_r(u)}, \qquad (8)$$
$$\bar{\mathbf{b}}_{i1}(v) = (1-\dot{\iota}_i)\bar{\mathbf{p}}_i(v) + \dot{\iota}_i\bar{\mathbf{p}}_{i+1}(v)\ ,$$
$$\bar{\mathbf{b}}_{i2}(v) = \dot{\tilde{\iota}}_i\bar{\mathbf{p}}_i(v) + (1-\dot{\tilde{\iota}}_i)\bar{\mathbf{p}}_{i+1}(v)\ ,$$
$$\bar{\mathbf{b}}_{i0}(v) = (1-\dot{\chi}_i)\bar{\mathbf{b}}_{i-1,2}(v) + \dot{\chi}_i\bar{\mathbf{b}}_{i1}(v),$$
$$\bar{\mathbf{b}}_{i-1,3}(v) = \bar{\mathbf{b}}_{i0}(v).$$

The proof then follows from Theorem 1. □

Using (7) and following the steps of the tensoring procedure, we get the following corollary.

Corollary 1 Considering one coordinate at a time, let $\{f_i(u)\}$ be the rational cubic pieces of a G^2 spline with control points $\dot{\mathbf{p}}_i$ as in Theorem 1; and let $\{g_j(v)\}$ be another piece with control points $\ddot{\mathbf{p}}_j$.
(a) Then the bi-cubic functions $f^{ij}(u,v) := f_i(u)g_j(v)$ form a bi-cubic rational G^2 spline with control points $\mathbf{p}^{ij} := \dot{\mathbf{p}}_i\ddot{\mathbf{p}}_j$.
(b) If all $\mathbf{p}^{ij} := 1$ then $f^{ij} \equiv 1$.

3.1. Reproduction of Basic Shapes

We consider several families of basic shapes. Many of these basic shapes have a natural trigonometric representation in real projective 3-space $\mathbb{P}^3$, i.e. equivalence classes of 4-tuples of real numbers. By re-representing cos-sin-pairs as rational G^2 cubics and applying Corollary 1, we will be able to express them as $d=4$-tuples of rational, scalar-valued coordinate maps f_k^{ij}, $k=1,2,3,4$ of type (6), with coefficients $\mathbf{b}_{rs,k}^{ij}\in\mathbb{R}$. Since the denominators of all four splines are identical, they are cancelled when we form the rational spline in $\mathbb{R}^3$ and since all f_{ij}^k share the same β, γ, the remark following Definition 1 guarantees G^2 continuity.

1. The first family to be reproduced has the homogeneous parameterization $(h_1,h_2,h_3,h_4)\in\mathbb{P}^3$ where

$$h_k := a_{k0}+a_{k1}\cos u+a_{k2}\sin u+a_{k3}\cos v+a_{k4}\sin v+ (a_{k5}\cos u+a_{k6}\sin u)\cos v+(a_{k7}\cos u+a_{k8}\sin u)\sin v. \quad (9)$$

This includes the torus and cyclides. For given partitions (opening angles) $\{\dot\alpha_i\}$ in the u-direction and $\{\ddot\alpha_j\}$ in the v-direction, we convert the cos-sin-pairs by (5), apply Corollary 1 and gather coefficients after scaling by a_{ks} to obtain the 4-tuples $(\mathbf{p}_1^{ij},\mathbf{p}_2^{ij},\mathbf{p}_3^{ij},\mathbf{p}_4^{ij})$ that the Bi-cubic Construction converts to the standard form (6).

2. The second family includes all quadric surfaces except for the hyperbolic paraboloid which appears in 3. In particular, the family includes the sphere with or without composition with Möbius transformations. Its $\mathbb{P}^3$ parameterization, for $k=1,2,3,4$, is

$$h_k := \sum_{s=0}^{3}(a_{ks0}+a_{ks1}\cos u+a_{ks2}\sin u)v^s. \quad (10)$$

For given opening angles in the u-direction, we convert the cos-sin-pairs by (5) and Corollary 1 into rational cubic G^2 form and set all v-direction weights to 1 so that $w_{rs}^{ij}:=\dot w_r^i$. The v-direction is treated as a spline by expressing v^s as a C^2 spline with knot sequence $\{v_j\}$. Then $\ddot\beta_j:=\frac{v_{j+1}-v_j}{v_j-v_{j-1}}$, $\ddot\gamma_j:=0$. We then combine with coefficients a_{ks} to obtain the 4-tuple $(\mathbf{p}_1^{ij},\mathbf{p}_2^{ij},\mathbf{p}_3^{ij},\mathbf{p}_4^{ij})\in\mathbb{R}^4$ which the Bi-cubic Construction converts to the standard form (6).

3. The third family has a bi-cubic homogeneous parameterization and includes the hyperbolic paraboloid. In general, we proceed as in 2 above. As a special case, we include a non-uniform bi-cubic polynomial spline by setting all weights to 1, $\dot\gamma_i:=0=:\ddot\gamma_j$ and all scalars $\dot\beta_i$, $\ddot\beta_j$ to the ratio of the lengths of consecutive knot intervals. The G^2 control mesh is the spline control net.

4. Design With G^2 Splines

Bi-cubic rational splines (6) offer a number of scalar and vector-valued parameters: $\dot w_r^i,\dot\beta_i,\dot\gamma_i$ and $\mathbf{b}_{rs}^{ij}$. In contrast to the classical algebraic treatment [Boe87, GB88,

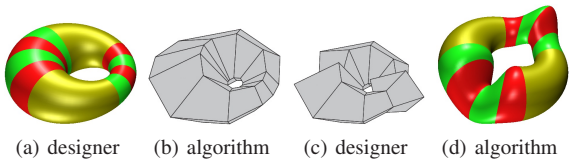

(a) designer (b) algorithm (c) designer (d) algorithm

Figure 5: *Design workflow: (a) the designer partitions, (b) the algorithm creates the mesh and sets the parameters, (c) the designer modifies, (d) the algorithm creates the surface.*

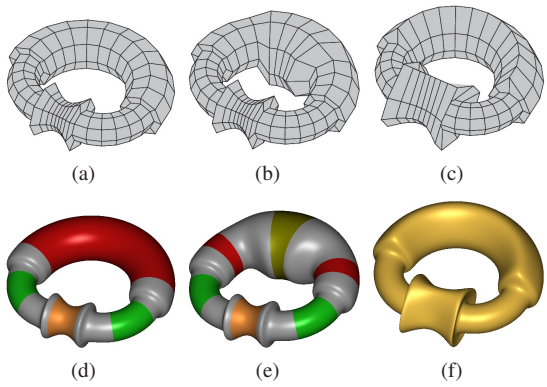

(a) (b) (c) (d) (e) (f)

Figure 6: *Alternative designs based on meshes of three torus segments (red and green in (d) and (e)) and of one one-sheeted hyperboloid (orange). The transitions are gray.*

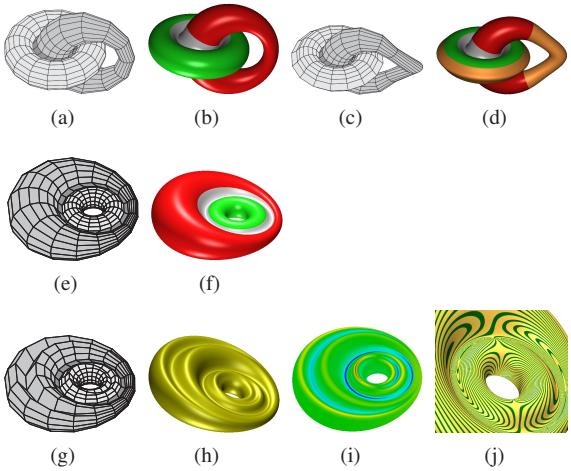

(a) (b) (c) (d) (e) (f) (g) (h) (i) (j)

Figure 7: *Alternative designs for joining a torus with a cyclide. Red and green regions remain as pieces of the original shapes; transitions are gray; (i) mean curvature of (h), (j) highlight lines (zoomed in).*

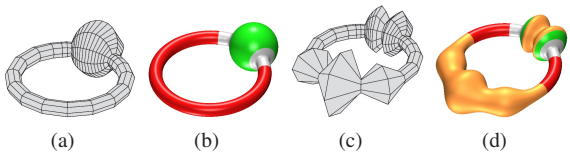

(a) (b) (c) (d)

Figure 8: *Designs appreciated in particular by very young audiences, joining a torus (red) with a sphere (green).*

Joe89, Bar93], here the designer is not expected to set these parameters. Rather, all parameters of the 4-tuples $(f_1^{ij}(u,v),\ldots,f_4^{ij}(u,v))$ are initialized to reproduce basic shapes (including bi-cubic NURBS) and modifying them is entirely optional. The suggested workflow is summarized in Fig. 5. In (a) the designer indicates a local region to work on, in (c) the designer manipulates the spline control points $(\mathbf{p}_1^{ij},\mathbf{p}_2^{ij},\mathbf{p}_3^{ij},\mathbf{p}_4^{ij})$ by standard CAD tools in 3-space as

$$\mathbf{a}^{ij} := \Big(\frac{\mathbf{p}_1^{ij}}{\mathbf{p}_4^{ij}},\frac{\mathbf{p}_2^{ij}}{\mathbf{p}_4^{ij}},\frac{\mathbf{p}_3^{ij}}{\mathbf{p}_4^{ij}}\Big)\in\mathbb{R}^3,\qquad \hat{W}^{ij} := \mathbf{p}_4^{ij}. \tag{11}$$

In return, the algorithm reverses (11) to obtain $\mathbf{p}^{ij}\in\mathbb{R}^4$ from $\mathbf{a}^{ij},\hat{W}^{ij}$, applies the Bi-cubic Construction to obtain new affine Bézier coefficients $b_{rs,k}^{ij}\in\mathbb{R}$, $k=1,\ldots,4$ and, since the 4-tuple of functions f_k^{ij} represents a function in $\mathbb{P}^3$, the common denominator can be discarded to obtain a 4-tuple of polynomial maps with control points

$$(w_{rs}^{ij}b_{rs,1}^{ij},w_{rs}^{ij}b_{rs,2}^{ij},w_{rs}^{ij}b_{rs,3}^{ij},w_{rs}^{ij}b_{rs,4}^{ij})\in\mathbb{R}^4$$

that define a rational bi-3 spline patch in $\mathbb{R}^3$.

Examples In the following examples, parts of the G^2 meshes $\{\mathbf{p}^{ij}\}$ of several basic shapes are merged into one G^2 mesh, without adding any control points! While more subtle transitions can potentially be designed by adding transition layers, the examples show that even straightforward use of the new spline representation yields satisfactory results.

Fig. 6 shows G^2 design variations that merge torus pieces with a one-sheeted hyperboloid. Fig. 7 shows G^2 design variations that merge a cyclide with a torus. Fig. 8 shows G^2 design variations that merge a torus with a sphere. Note that the cut torus piece does not meet the sphere at axially symmetric points. Changing the location of the poles, by a Möbius transformation, will be addressed in the next section.

5. Free-form Sphere-Based Design

To allow design variations, the sphere is re-represented as a bi-cubic G^2 spline patchwork where the patches surrounding the poles form a specially constructed assembly of bi-cubic patches with one edge collapsed to the pole. This explicit singularity is acceptable to CAD packages and allows for much lower degree than the construction in [BP97].

5.1. Polar Construction

As illustrated in Fig. 9 (a), (b), the control mesh of our construction is a regular tensor-product mesh with control points collapsed to form a northern and a southern triangle fan, called *polar configurations* [KP09]. Apart from these configurations, the algorithm of Section 3.1 applied to the (gray) mesh in Fig. 9 (a) yields the equatorial part of the sphere shown in Fig. 9 (c). Interpreting the carefully-set polar control points as collapsed edges and choosing the proper scalar

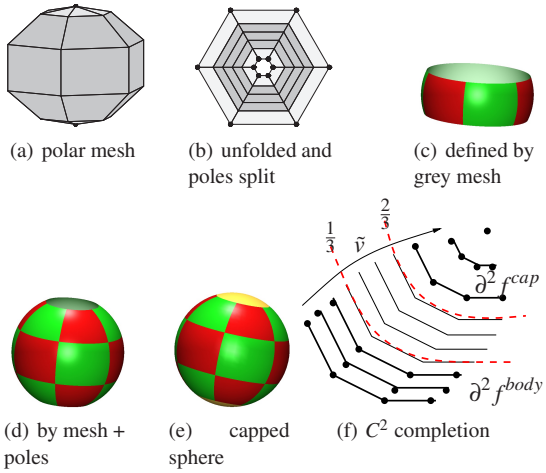

Figure 9: Bi-cubic spline sphere. *(a) and (b) Control mesh with polar configuration. (f) Logical diagram (layers of control points) of a C^2 completion of a 3-piece polar cap.*

parameters in the pole-to-pole direction (see General Construction at Poles below) the algorithm yields the additional sphere-reproducing spline rings of Fig. 9 (d).

To exactly reproduce a spherical cap, we reparameterize the inverse stereographic projection $\mathfrak{s}^{-1} := (2x,2y,1-x^2-y^2,1+x^2+y^2)\in\mathbb{P}^3$ by $(x(u,v),y(u,v)) = \rho(u,v)$

$$\rho(u,v) := \Big(\frac{1-v}{v}\cos u,\frac{1-v}{v}\sin u\Big). \tag{12}$$

That is, we form $\mathfrak{s}^{-1}(\rho)$ where $v=0$ corresponds to south pole and $v=1$ to the north pole. Multiplication by v^2 clears the common denominators of the 4-tuple to yield a rational bi-3 G^2 spline.

General Construction at Poles For the south-to-north direction parameterized by v, we pick the knot sequence $[0,v_1,\ldots,v_m,1]$, scalars β_0, β_{m+1}, $\gamma_0=0=\gamma_{m+1}$ and the polar control points

$$\begin{aligned}\mathbf{p}^{\text{south}} &:= (0,0,\frac{3-3v_1+2v_1^2}{3(v_1-1)},1)\ ,\ \beta_0 := 1-v_1,\\ \mathbf{p}^{\text{north}} &:= (0,0,\frac{2-v_m+2v_m^2}{3v_m},1)\ ,\ \beta_{m+1} := \frac{1}{v_m}.\end{aligned} \tag{13}$$

We construct the polar caps so that the free-form G^2 bi-cubic spline defaults to the sphere (Fig. 9 (e)). A polar spline cap is periodic in u. In v, it is partitioned into three C^2-connected rings with the outer ones interpolating, respectively, data at the pole and of the existing body (Fig. 9 (f)). The expansion at the pole is obtained by generalizing $\mathfrak{s}^{-1}$ to

$$\begin{aligned}\mathfrak{q} &:= (\mathfrak{q}_1,\mathfrak{q}_2,\mathfrak{q}_3,\mathfrak{q}_4)\in\mathbb{P}^3,\\ \mathfrak{q}_k &:= q_{k0}+q_{k1}x+q_{k2}y+q_{k3}(x^2+y^2),\end{aligned} \tag{14}$$

with, as yet, undetermined coefficients q_{ks} and form

$$\mathfrak{q}(\mathfrak{p}(u, v_m(1-\tilde{v})+\tilde{v})), \quad \tilde{v} \in [0..1]. \tag{15}$$

As before, we replace the $\sin u$, $\cos u$ pairs in this expression by (5) and remove the common denominator of the 4-tuple. This yields a bi-2 map that is expressed in our bi-cubic form as f^{cap}. We determine the coefficients q_{ks} so that the boundary of the bi-cubic cap best matches the boundary of the already constructed bi-cubic patches f^{body} of Fig. 9 (d). Concretely, we minimize the two-norm distance of position, first and second derivative, i.e. the 2-jet along the boundary, $\partial^2 f^{body}$. As a reparameterization of a quadratic, the constructed bi-cubic cap is infinitely smooth at the pole, but typically does not join smoothly with f^{body}. A simple remedy is to trisect the cap in the v direction and have the sub-patches adjacent to f^{body} inherit its 2-jet (Fig. 9 (f)). Then the 2-jets of f^{cap} and f^{body} uniquely determine the remaining Bézier coefficients since we require that the patches join parametrically C^2 as 4-tuples in the v direction.

Since the map $\mathfrak{q}$ can in particular represent $\mathfrak{s}^{-1}$, the cap construction completes a sphere if the data $\partial^2 f^{body}$ come from a sphere.

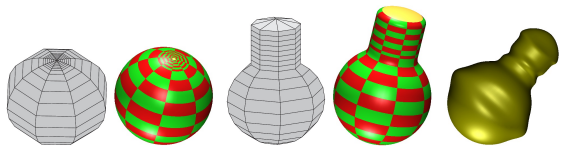

(a) sphere (b) merged with cylinder (c) design

Figure 10: Design with poles *(a) Mesh segmented to admit (b) merging with cylinder mesh; (d) design variation.*

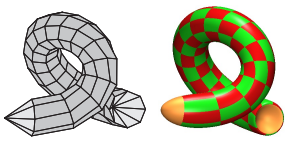

(a) (b)

Figure 11: Design with poles *Tube-design.*

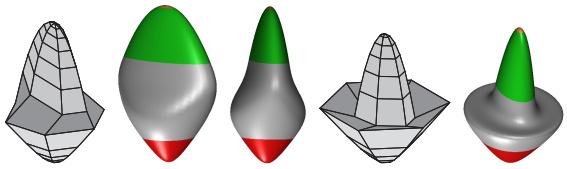

(a) (b) (c) (d) (e)

Figure 12: *Elliptic paraboloid (green) merged with a two-sheeted hyperboloid (red) into a smooth whole. (b) and (c) show two different viewpoints.*

Fig. 11 illustrates the capping of NURBS tubes of degree bi-3 with caps of degree bi-3. Note for comparison that the algorithm in [KP09] results in a cap of degree 6 in the u-direction. An analogous capping procedure applies to the elliptic paraboloid and the two-sheeted hyperboloid as shown in Fig. 12.

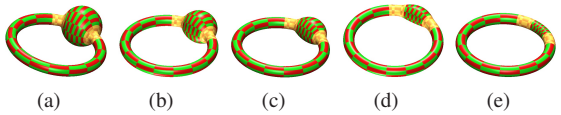

(a) (b) (c) (d) (e)

Figure 13: *Morphing the sphere-torus G^2 spline (a) of Fig. 8 to a single torus (e).*

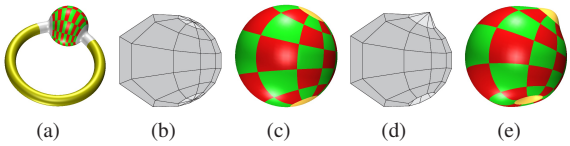

(a) (b) (c) (d) (e)

Figure 14: Möbius transformation for free-form spheroids. *(a) Bi-cubic patchwork on sphere of the surface from Fig. 8. (b) polar mesh of sphere stemming from composition of $M(z)$ with inverse of stereographic projection. (c) corresponding bi-cubic patchwork of sphere. (d) perturbed polar mesh. (e) perturbed spheroid.*

While for typical design, the initial choice of scalars $\dot{w}^i_r, \dot{\beta}_i, \dot{\gamma}_i$ and $\ddot{w}^j_s, \ddot{\beta}_j, \ddot{\gamma}_j$ are defined to reproduce the basic shapes in Section 3.1 and need not be modified, they and the control points can be continuously changed to morph between basic shapes, as in Fig. 13.

Möbius transformations Figures 8 and 14 demonstrate the need for controlling the placement of poles for design with sphere-like free-form shapes: the ends of the cut torus do not meet the sphere at opposing points. To adjust poles, we use the Möbius transformation of the sphere, a composition of the stereographic projection $\mathfrak{s}$ with the rational linear mapping $M(z) := \frac{az+b}{cz+d}$, $z = x + \sqrt{-1}y$ and the inverse stereographic projection: $\mathfrak{s} \circ M \circ \mathfrak{s}^{-1}$. For our application, we can restrict $M(z) := \frac{z+b}{bz+1}$, $b \in \mathbb{R}$ which moves the north pole to $\left(\frac{2b}{1+b^2}, 0, \frac{1-b^2}{1+b^2}\right)$ and the south pole to $\left(\frac{2b}{1+b^2}, 0, -\frac{1-b^2}{1+b^2}\right)$.

In general, we compose $\mathfrak{q} \circ M \circ \mathfrak{p}$ to obtain for each coordinate (hence dropping the index k)

$$\begin{aligned}\mathfrak{q} :=& q_0 b^2 + q_1 b + q_3 + \big(q_1\mathsf{c} + q_2\mathsf{s} - 2q_3 \\ &+ 2(q_0\mathsf{c} - q_1 + q_3\mathsf{c})b - (2q_0 - q_1\mathsf{c} + q_2\mathsf{s})b^2\big)v \\ &+ \big(q_0 - q_1\mathsf{c} - q_2\mathsf{s} + q_3 - 2(q_0\mathsf{c} - q_1 + q_3\mathsf{c})b \\ &+ (q_0 - q_1\mathsf{c} + q_2\mathsf{s} + q_3)b^2\big)v^2,\end{aligned}$$

where $\mathsf{c} := \cos u$, $\mathsf{s} := \sin u$. With the scalars β_i, γ_i of (13)

$$\begin{aligned}\mathbf{p}^{\text{south}} &:= (2b, 0, \frac{(1-b^2)(3-3v_1+2v_1^2)}{3(v_1-1)}, 1+b^2),\\ \mathbf{p}^{\text{north}} &:= (2b, 0, \frac{(1-b^2)(2-v_m+2v_m^2)}{3v_m}, 1+b^2)\end{aligned} \tag{16}$$

generalizes (13).

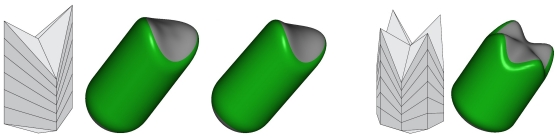

(a) saddle mesh (b) $\mathfrak{q}$ (c) general (d) 4-saddle, $\mathfrak{q}$

Figure 15: *Non-elliptic cappings of cylinder.*

Saddle-like Polar Constructions Polar configurations are typically used with elliptic designs. For completeness, we consider here the hyperbolic case. The mesh in Fig. 15 (a) calls for a saddle. The construction using $\mathfrak{q}$ of the form (14) results in the oscillating surface (b). This can be repaired to obtain (c), by replacing $\mathfrak{q}$ with a general quadratic with six coefficients per coordinate, at the cost of increasing the bi-degree to 4. On the other hand, $\mathfrak{q}$ works well for higher-order saddles that have central points with zero curvature (d).

6. Conclusion

We created an analogue of tensor-product C^2 bi-cubic splines, the workhorse of CAD geometry processing, in order to exactly reproduce parts of the classical shapes automatically joined into a smooth whole. This opens up a number of applications in design, localized re-design or reconstruction in reverse engineering (see e.g. [BMV01, AJS11]). An analogous rational bi-2 G^1 spline construction generalizes C^1 bi-2 splines but yields surfaces of lower quality.

Extending the approach to more general settings such as in Fig. 16, requires multi-sided blends that lead to splines of higher degree than bi-3, with additional techniques outside the scope of this presentation. Subdividing the splines can be used to localize deformations, but also gives a first subdivision algorithm able to combine basic shapes in one smooth whole.

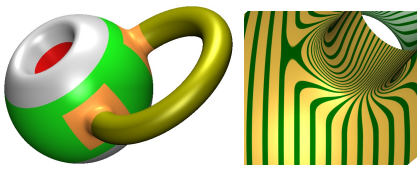

(a) (b) reflection lines

Figure 16: *G^2 multi-sided blend of degree bi-6.*

We focused on the use of splines to support conceptual design, starting from primary shapes that represent functionality or simplicity of shape. Since portions of the basic shapes are reproduced exactly, the spline constructions can also be viewed as a form of interpolation.

The approach taken is novel in the way it combines G^2 continuity and projective trigonometric parameterizations. The classical work, on rational spline curves [Boe87, GB88, Joe89, Bar93] and surfaces [ZWL92, ZWL95], focused on general necessary and sufficient constraints for smoothness but missed out on the specific useful constructions we presented here. Only looking for and finding formulas such as (4) allows combining the exact pieces smoothly – which may explain why no such construction existed to date.

References

[AJS11] ANDREWS J., JOSHI P., SÉQUIN C.: Interactive extraction and re-design of sweep geometries. In *Computer Graphics International* (2011), W. Lee N. M.-T., Stam J., (Eds.), p. to appear. 7

[Bar93] BARSKY B. A.: Rational beta-splines for representing curves and surfaces. *IEEE Computer Graphics and Applications 13*, 6 (Nov. 1993), 24–32. 1, 4, 7

[BMV01] BENKÖ P., MARTIN R. R., VÁRADY T.: Algorithms for reverse engineering boundary representation models. *Computer-Aided Design 33*, 11 (2001), 839–851. 7

[Boe87] BOEHM W.: Rational geometric splines. *Computer Aided Geometric Design 4*, 1-2 (July 1987), 67–77. 1, 4, 7

[BP97] BANGERT C., PRAUTZSCH H.: Circle and sphere as rational splines. *Neural, Parallel and Scientific Computations*, 5 (1997), 153–162. 2, 5

[Far88] FARIN G.: *Curves and Surfaces for Computer Aided Geometric Design: A Practical Guide*. Acad. Press, 1988. 2, 3

[GB88] GOLDMAN R. N., BARSKY B. A.: *Beta Continuity and Its Application to Rational Beta-splines*. Technical Report CSD-88-442, UC Berkeley, Aug. 1988. 1, 4, 7

[Joe89] JOE B.: Multiple-knot and rational cubic beta-splines. *ACM Transactions on Graphics 8*, 2 (1989), 100–120. 1, 4, 7

[KP] KARČIAUSKAS K., PETERS J.: Rational G^2 splines. *Graphical Models*, 1–23. in press. 2

[KP09] KARČIAUSKAS K., PETERS J.: Finite curvature continuous polar patchworks. In *IMA Mathematics of Surfaces XIII* (2009), Hancock E., Martin R., (Eds.), pp. 222–234. 5, 6

[PBP02] PRAUTZSCH H., BOEHM W., PALUSZNY M.: *Bézier and B-spline techniques*. Springer, 2002. 2

[ZWL92] ZHENG J., WANG G., LIANG Y.: Curvature continuity between adjacent rational Bézier patches. *Comp Aided Geom Design 9*, 5 (1992), 321–335. 7

[ZWL95] ZHENG J., WANG G., LIANG Y.: GC_n continuity conditions for adjacent rational parametric surfaces. *Comp Aided Geom Design 12*, 2 (1995), 111–129. 7

Acknowledgement This work was supported in part by NSF Grant CCF-0728797.